Brain, Behavior, and Immunity 93 (2021) 299–311

Contents lists available at ScienceDirect

Brain Behavior and Immunity

journal homepage: www.elsevier.com/locate/ybrbi

Full-length Article

Plasma-derived and recombinant C1 esterase inhibitor: Binding profiles and neuroprotective properties in brain ischemia/reperfusion injury

Domenico Mercurio [a,1], Arianna Piotti [b,1], Alessia Valente [a], Marco Oggioni [a], Yolanda Ponstein [c], Edwin Van Amersfoort [c], Marco Gobbi [b], Stefano Fumagalli [a,*], Maria-Grazia De Simoni [a]

[a] Istituto di Ricerche Farmacologiche Mario Negri IRCCS, Department of Neuroscience, Milan, Italy
[b] Istituto di Ricerche Farmacologiche Mario Negri IRCCS, Department of Biochemistry and Molecular Pharmacology, Milan, Italy
[c] Pharming Technologies B.V., Leiden, The Netherlands

ARTICLE INFO

Keywords:
C1 inhibitor
Complement system
Mannose-binding lectin
Stroke

ABSTRACT

C1 esterase inhibitor (C1INH) is known to exert its inhibitory effect by binding to several target proteases of the contact and complement systems. One of C1INH's targets comprise mannose-binding lectin (MBL), a critical player in post-stroke pathophysiology. We therefore explored the effects of recombinant human (rh) and plasma derived (pd) C1INH in C57BL/6J mice subjected to transient occlusion of the middle cerebral artery (tMCAo), receiving 15 U/mouse of pd or rhC1INH intravenously, at reperfusion. We analyzed the compounds' (i) neuroprotective effects, (ii) plasma presence, (iii) effects on circulating and brain MBL, (iv) time course of endothelial deposition, and (v) effects on the formation of active complement products. rhC1INH-treated mice had neuroprotective effects, including reduced behavioral deficits and neuronal loss, associated with decreased MBL brain deposition and decreased formation of complement C4b active fragments. In contrast, pdC1INH did not show these neuroprotective effects despite its longer plasma residence time. We also analyzed the response to tMCAo in C1INH-deficient mice, observing a poorer ischemic outcome compared to the wild type mice, which could be partially prevented by rhC1INH administration.

In conclusion, we show that rhC1INH exhibits stronger neuroprotective effects than the corresponding plasma-derived protein after experimental ischemia/reperfusion injury in the brain, placing it as a promising drug for stroke. Differential effects are likely related to more effective MBL inhibition which further confirms it as a useful pharmacological target for stroke.

1. Introduction

Stroke treatment improved since the advent of mechanical thrombectomy and recanalization techniques, but, due to treatment restrictions, the majority of stroke patients cannot benefit from these novel approaches (Hacke, 2015). In the search of new therapeutic strategies with a wide window of efficacy, pre-clinical research has focused on inflammation (Lambertsen et al., 2019), hallmark of stroke in humans and in animal models. Stroke elicits inflammatory mechanisms both locally in the brain (Wimmer et al., 2018) and systemically (Krishnan and Lawrence, 2019), offering multiple targets, i.e. circulating immune cell populations (Cramer et al., 2019) as well as brain endothelium (Andjelkovic et al., 2019). The activation of the complement cascade has a prominent role, coordinating multiple thromboinflammatory events occurring on the brain ischemic endothelium and contributing to lesion expansion (i.e. neuronal loss) over time (Orsini et al., 2018). As such, pharmacological targeting of the complement system appears a promising strategy to alleviate stroke pathological *sequelae*. Notably, compounds effectively inhibiting the complement cascade that are approved for clinical use, or in phase 3 trials, for other pathologies, lend support to their rapid clinical transferability if proven effective for stroke treatment.

C1 inhibitor (C1INH), a glycoprotein that acts as a regulator of among others the complement system, is one of the clinically available compounds. The recombinant human (rhC1INH) and plasma derived (pdC1INH) products are used to treat acute attacks in patients with hereditary angioedema (HAE), a rare disease caused by partial C1INH deficiency. Furthermore, C1INH was also proven effective in reducing

* Corresponding author.
E-mail address: stefano.fumagalli@marionegri.it (S. Fumagalli).
[1] Equal contribution

https://doi.org/10.1016/j.bbi.2021.01.002
Received 29 September 2020; Received in revised form 23 December 2020; Accepted 6 January 2021
Available online 11 January 2021

behavioral outcome and lesion size in experimental stroke. Using a mouse model of ischemia/reperfusion injury (IRI), achieved by 30 min occlusion of the middle cerebral artery, our group previously reported a wider therapeutic window of efficacy for rhC1INH than pdC1INH (up to 18 h compared to <6 h) (Gesuete et al., 2009). This data was obtained despite a significant shorter plasma half–life of rhC1INH than pdC1INH, as identified in the clinical HAE setting. The different pharmacokinetics of recombinant and plasma C1INH may depend on the differences in glycosylation, resulting in different receptor binding profile (Farrell et al., 2013; van Doorn et al., 2005).

In the previously mentioned mouse model we also reported a higher ability of rhC1INH compared to pdC1INH to deposit on the ischemic endothelium, with the latter shown to extravasate (Gesuete et al., 2009). In addition, and in line with a difference in glycosylation binding profile, previous data supported a higher ability of rhC1INH compared to pdC1INH to target, *in vitro*, the lectin complement pathway (LP). The present study aimed at extending the data on rhC1INH mechanism of action in the *in vivo* model of ischemia/reperfusion injury, with particular focus on the targeting of the LP. In fact, among the complement activation pathways, the LP was reported to provide the wider contribution to ischemic stroke pathophysiology, both in experimental models and humans (Fumagalli and De Simoni, 2016). Mannose-binding lectin (MBL) is one of the LP initiator molecules, reported to be at crossroads of pathophysiological events after stroke, including inflammation enhancement, inflammatory activation of platelets, microvascular leakage (de la Rosa et al., 2014), alterations of hemodynamics, increases in endothelial adhesion molecule expression (Orsini et al., 2018) and direct endothelial structural damage (Neglia et al., 2020a). The two MBL murine isoforms – MBL-A and MBL-C – were seen deposited on the brain vessels pertinent to the ischemic territory, starting as early as 6 h after the insult (Neglia et al., 2020b; Orsini et al., 2012). Inhibiting MBL's deposition correspondingly provided neuroprotection after experimental stroke in mice (Orsini et al., 2012).

This study aims at assessing the neuroprotective properties of C1INH and further investigate the mechanism of action, localization and effectiveness in inhibiting MBL. We administered pd or rhC1INH to brain ischemic mice, and analyzed their (i) neuroprotective effects, (ii) plasma presence, (iii) effects on circulating and brain MBL, (iv) time course of endothelial deposition, and (v) effects on the formation of active complement products. We showed the superior protective effects of rhC1INH after experimental ischemia and reperfusion injury which were linked to an effective LP inhibition. Finally, we also showed rhC1INH beneficial effects in brain ischemia in C1INH-deficient mice.

2. Materials and methods

2.1. Mice

Procedures involving animals and their care were conducted in conformity with institutional guidelines in compliance with national and international laws and policies. Ethical approval to animal procedures was obtained from the internal Ethical Committee at the Istituto di Ricerche Farmacologiche Mario Negri IRCCS and from the Italian Ministry of Health (authorization number 224/2016-PR).

We used male C57BL/6J wild type (WT, purchased from Charles Rivers-Italy). In addition, we used male C57BL/6N mice that were C1INH deficient and the corresponding C57BL/6N wild type mice, both provided by Taconic Biosciences on behalf of Pharming Technologies B. V. The generation of the constitutive C1INH knock-out (KO) mouse model was accomplished by editing the *Serping1* gene via the CRISPR/Cas9 method and introducing a deletion of exon 3. The targeting strategy was based on NCBI transcript NM_009776.3 and the Cas9 protein along with the proximal and distal guide RNAs (gRNAs) were injected in C57BL/6NTac zygotes. Founder (F0) animals were subsequently bred to C57BL/6NTac animals to obtain heterozygous (HET) animals and a single founder line was used for further expansion and intercrossing to generate animals for experiments. To analyze the vascular anatomy of C1INH KO mice, we stained vessels as described previously (Orsini et al., 2016; Perego et al., 2019). Briefly, mice were transcardially perfused with PBS 0.1 mol/L followed by a mixture of two commercially available inks, Pelikan Stempelfarbe ink and Pelikan calligraphy ink (1:9, respectively). Brains were then removed and fixed overnight with 4% paraformaldehyde. Ink-stained brains from C57BL/6N WT and C1INH KO mice were positioned on graph paper and a picture was taken from above. Image processing was performed using ImageJ software. The anastomotic line between the MCA and anterior carotid artery was drawn blindly and the distance between the brain midline and the anastomotic line was measured at 4 and 6 mm distance from the frontal pole.

During the experiments, mice were 9–11 weeks old, with a body weight of 20–30 g. The protocols and details of this study are in accordance with the ARRIVE guidelines (http://www.nc3rs.org.uk/page.asp?id=1357, see the list provided as a supplementary file). We used only male mice since estrogens affect ischemic outcome in experimental models, which could interfere with interpretation of the results (Carswell et al., 2009).

2.2. Focal cerebral ischemia

2.2.1. Surgery

Focal cerebral ischemia was induced by transient middle cerebral artery occlusion (tMCAo) as previously reported by our group (Neglia et al., 2020b). Anesthesia was induced by 3% and maintained by 1.5% isoflurane inhalation in an N_2O/O_2 (70/30%) mixture. Transient ischemia (60 min) was achieved using the filament model. A silicone coated monofilament nylon suture (sized 7–0, diameter 0.06–0.09 mm, length 20 mm; diameter with coating 0.23 mm; coating length 10 ± 1 mm, Doccol Corporation, Redlands, CA, USA) was introduced into the common carotid artery (appropriately isolated) and advanced to block the middle cerebral artery (MCA). After 60 min, blood flow was restored by carefully removing the filament. During surgery body temperature was kept at 37 °C by a heating pad. During MCA occlusion, mice were awakened from anesthesia, kept in a warm box and tested for intraischemic deficits (for inclusion/exclusion criteria, see below). Analgesia was achieved by local application of an ointment (EMLA, containing 2.5% lidocaine and prilocaine, Aspen Pharma) where the skin was opened. Animals were monitored after surgery according to the IMPROVE guidelines (Percie du Sert et al., 2017) and treated subcutaneously with 0.1 mg/kg buprenorphine if developing severe signs of distress (IMPROVE's amber category of clinical signs). Surgery-associated mortality was below 2%, see Supplementary Table S1.

2.2.2. Inclusion/exclusion criteria

Mice were included in the study if successfully induced with ischemia, i.e. filament correctly positioned in the MCA. Thus, ischemic animals were included if presenting ≥3 of the following intraischemic deficits:

1. the palpebral fissure had an ellipsoidal shape (not the normal circular one)
2. one or both ears extended laterally
3. asymmetric body bending on the ischemic side
4. limbs extended laterally and did not align to the body.

Mice were excluded if:

1. they died during MCA surgery
2. they had a decrease in body weight >35% before sacrifice compared to baseline

Supplementary Table S1 shows the results of the above-mentioned analysis to include mice into the evaluation.

2.3. Treatments

Mice received by intravenous (IV) bolus injection in the tail vein at reperfusion, while still under anesthesia, 15 U/mouse pdC1INH or rhC1INH or saline (injected volumes maximally 150 μL/mouse). The test items were stored at −80 °C until use. rhC1INH and pdC1INH were provided by Pharming.

2.4. Behavioral deficits

Two days after tMCAo, each mouse underwent neuroscore evaluation for assessment of sensorimotor deficits. Scores ranged from 0 (healthy) to 56 (worst performance) combining general and focal deficits. The complete list of assessed parameters was published in Llovera et al. (Llovera et al., 2015).

2.5. Plasma collection, sacrifice and tissue collection

Mice were anesthetized with 300 μL of ketamine (150 mg/kg) plus medetomidine (2 mg/kg) intraperitoneally before sacrifice.

2.5.1. Plasma collection

Blood (≈400 μL) was obtained from the right ventricle with a syringe containing EDTA-polybrene to prevent coagulation. Blood was centrifuged at 2000 g for 15 min at 4 °C and the plasma was stored at −80 °C for subsequent analyses.

2.5.2. Brain collection

Mice were transcardially perfused with 30 mL of phosphate buffered saline (PBS) 0.1 mol/L, pH 7.4, followed by 60 mL of chilled paraformaldehyde (4%) in PBS. The brains were carefully removed from the skull and post-fixed for 6 h at 4 °C, then transferred to 30% sucrose in 0.1 mol/L phosphate buffer for 24 h until equilibration. The brains were frozen by immersion in isopentane at −45 °C for 3 min and stored at −80 °C until use.

2.6. Ischemic volume assessment

Twenty-μm coronal brain cryosections were cut serially at 320 μm intervals and stained with cresyl violet. The infarcted area was delineated by the relative paleness of histological staining, tracing the area using ImageJ software. The infarcted area was corrected for edema (percentage of swelling based on the difference between ipsi- and contralateral sides). Infarct volumes were calculated by the integration of infarcted areas on each brain slice (Perego et al., 2011).

2.7. Neuronal density

Three cresyl violet–stained 20 μm-thick coronal sections at −0.6, 0 and + 0.6 mm from the bregma were acquired from each mouse and visualized at 20× magnification with an Olympus BX61 Virtual Stage microscope, with a pixel size of 0.346 mm. Neuronal counting was performed by segmenting the cells in regions of interest designed in the cortex and striatum where the lesion was clearly detectable. The regions of interest on the contralateral side were positioned mirroring those on the ipsilateral side. A segmented circular signal smaller than the area threshold of 25 μm^2, which is associated with glial cells was excluded from the analysis (supplementary Fig. S1). For quantification, we used ImageJ software (Schindelin et al., 2012) and neuronal cell number was expressed as neuronal density (cell/mm^2) in the ipsi- and contralateral regions of interest.

2.8. TUNEL staining and quantification

Apoptotic cells were labeled by in situ cell death detection kit (Roche, Mannheim, Germany). TUNEL negative control was done by omitting the enzyme during the reaction. TUNEL positive control was done by treating the samples with 1 μg/mL DNAse. TUNEL was acquired with a 20× 0.5NA objective (pixel size 0.62 μm) by an A1 Nikon confocal microscope, by using excitation wavelength at 561 nm. Acquisition was performed on a brain section at −1.5 mm from bregma. Three-dimensional volumes sized 635 × 635 × 20 μm (striatum), 1779 × 635 × 20 μm (cortex) and 1779 × 1779 × 20 μm (hippocampus) were acquired with a 2.65 μm step size, with automatic stitching of single fields of view. The quantification of TUNEL positive cells microphotographs was done by ImageJ. Briefly, trainable Weka segmentation was used to identify TUNEL cells. A probability image was then created and only signal with >80% of probability of being actual TUNEL signal was quantified. The number of cell per brain area was calculated and used for statistical analysis (cell density).

2.9. Surface plasmon resonance studies

The surface plasmon resonance (SPR) apparatus used for all these analyses was a ProteOn XPR36 Protein Interaction Array system (Bio-Rad Laboratories, Hercules, CA), equipped with six parallel flow channels that can immobilize up to six ligands on the sensor chip surface. A summary of the main steps of the protocols used to detect human C1INH (hC1INH) or murine MBL isoforms in the plasma of treated mice is depicted in Supplementary Fig. S1.

The first step is the covalent immobilization on the sensor chip of antibodies against MBL-A/C (Hycult Biotech) or against hC1INH (Dako). Antibodies were immobilized by classical amine coupling chemistry (Beeg et al., 2019), flowing them on activated GLC sensor chips (Bio-Rad) for 5 min at a rate 30 μg/ml in acetate buffer pH 5. In parallel surfaces of the same chip, we immobilized BSA (Sigma) or IgG (Sigma) (30 μg/mL for 5 min in acetate buffer pH 4.5 and pH 5, respectively) to be used for reference.

After the first immobilization step, the ProteOn XPR36 fluidic system was rotated 90° so that up to six different samples could be injected simultaneously over the immobilized ligands (Supplementary Fig. S1). In this second step, we injected mice plasma diluted 50-fold in 10 mM Tris buffer containing 1.2 mM $CaCl_2$, 150 mM NaCl, and 0.005% Tween 20, pH 7.4 (TBST/Ca^{2+}) (Beeg et al., 2019; Stravalaci et al., 2016). The running buffer was TBST/Ca^{2+}. With this second step, MBL or hC1INHs are captured onto the chip by the corresponding antibodies. The subtraction of the non-specific SPR signal detected, in parallel, on the reference surfaces (BSA or IgG), and due to plasma components, allows to determine the binding specifically due to MBL isoforms or hC1INH (Supplementary Fig. S2).

A third step was then added to enhance the specificity of – and amplify – the SPR signals (Canovi et al., 2014; Stravalaci et al., 2016). For this, after a further rotation of the fluidic system, we injected 10 μg/mL of the secondary antibodies, e.g. anti-hC1INH onto the surfaces where C1INHs present in mouse plasma were captured by immobilized anti-hC1INH.

All SPR assays were run at a rate of 30 μL/min at 25 °C. The sensorgrams (time course of the SPR signal in RU) were normalized to a baseline of 0.

2.10. Microglia/macrophage immunohistochemical analysis

Immunohistochemistry was performed on 20 μm brain coronal sections using rat anti-mouse CD11b (1.25 μg/mL, Bio rad, USA) followed by biotinylated anti-rat secondary antibody (7.5 μg/mL Vector Laboratories, USA). Positive cells were stained by reaction with 3,3′–diaminobenzidinetetrahydrochloride (DAB, Vector laboratories). For negative control staining, the primary antibody was omitted, and no staining was observed. Three 20 μm-thick coronal sections −0.6, 0 and + 0.6 mm from the bregma were acquired for each mouse at 20× with an Olympus BX61 Virtual Stage microscope, with a pixel size of 0.346 mm. The CD11b signal was segmented over the ischemic ipsilateral striatum

with ImageJ software (Schindelin et al., 2012). Segmented objects were also superimposed on a grid image with horizontal and vertical lines distanced by 9 μm. The total number of objects crossing on the grid was quantified and normalized for the total number of segmented objects. Data was expressed as percentages of stained area in the total area (Perego et al., 2011), circularity and grid touchings (Zanier et al., 2015).

2.11. C1INH immunofluorescence and quantification

Immunofluorescence was done on 20 μm coronal brain sections. After blockade with 3% normal goat serum for 1 h, sections were incubated with polyclonal rabbit α-human C1INH (5.8 μg/mL, A0253, Dako) primary antibody followed by biotinylated secondary anti-rabbit IgG antibody. Fluorescent signal was coupled using the TSA amplification kit (FITC, Perkin Elmer). Confocal microscopy was done using a sequential scanning mode to avoid bleed-through effects with a Nikon A1 confocal scan unit. Acquisition was done using the 20× objective to obtain fields of view sized 1170 × 1170 × 20 μm, located in the cortical ischemic area on sections at 1 and −1.5 mm from bregma. In order to quantify the signal for C1INH, the integrated density of the gray level value for the total C1INH signal in the ischemic areas was quantified. The integrated density was normalized on the total area (μm^2) occupied by the vessels. Images were finally elaborated and evaluated with ImageJ and GIMP.

2.12. MBL-C immunofluorescence and quantification

Immunofluorescence was done on 20 μm coronal brain sections. After blockade with 10% normal goat serum for 1 h, sections were incubated with rat anti-MBL-C (1 μg/mL; Hycult, No. HM1038) primary antibodies followed by Alexa 594-conjugated secondary antibodies raised in goat (4 μg/mL; Life Sciences). Blood vessels were visualized with Griffonia Simplicifolia isolectin B4 Alexa 488-conjugated (10 μg/mL; Life Sciences). For negative control staining, the primary antibodies were omitted, and no staining was observed. Confocal microscopy was done using a sequential scanning mode to avoid bleed-through effects with an Olympus FV500 microscope. Three-dimensional volumes were acquired over 7 to 10 μm stacks, with 0.23 μm step size. For the quantification of MBL-C staining, microphotographs were taken in the ischemic cortex (40x magnification, pixel size 0.45 μm) and processed by ImageJ. Briefly, a region of interest was delineated on the IB4 signal (blood vessels). The region of interest was then applied to the corresponding image with the MBL-C signal after appropriate normalization (the background noise was corrected by subtracting the mean pixel density of unstained areas). The integrated density was calculated and used for statistical analysis.

2.13. Fibrin(ogen) immunofluorescence and quantification

Immunofluorescence was done on 20 μm coronal brain sections. After blockade with 1% bovine serum albumin for 30 min, sections were incubated with a polyclonal rabbit α-human fibrin(ogen) FITC-conjugated antibody (42 μg/ml, F0111, Dako). For negative control staining, the primary antibody was omitted, and no staining was observed. Confocal microscopy was done using a sequential scanning mode to avoid bleed-through effects with an A1 Nikon confocal microscope. Three-dimensional volumes sized 1485 × 1485 × 20 μm were acquired with a 2.65 μm step size, with automatic stitching of single fields of view. For the quantification of fibrin(ogen) staining, microphotographs were taken in the ischemic cortex (20× magnification, 0.5NA objective, pixel size 0.62 μm) and processed by ImageJ. Briefly, trainable Weka segmentation was used to identify fibrin(ogen) positive signal with a vascular morphology. A probability image was then created and only signal with >80% of probability of being actual fibrin (ogen) was quantified. The area fraction (% area) occupied by the positive signal was calculated and used for statistical analysis.

2.14. Western blot analysis

Blood samples were collected in 10 mM ethylendiamine tetracetic acid and 0.125% polybrene (SigmaAldrich) and plasma was separated by centrifugation for 15 min at 2000 g at 4 °C and immediately stored at −80 °C. Equal amounts of plasma proteins (10 μg/sample) were electrophoresed on 12% sodium dodecyl sulfate polyacrylamide gel and transferred to polyvinylidene fluoride membranes. Rabbit anti-C3 polyclonal (0.32 μg/mL; Novus Biologicals) or rat anti-thrombomodulin monoclonal (1 μg/mL; R&D) antibody followed by anti-rabbit or anti-rat peroxidase-conjugated antibodies (respectively 0.16 μg/mL, Santa Cruz Biotechnology or 0.1 μg/mL; abcam) were used. To measure the level of C4b the polyvinylidene fluoride membranes were previously incubated for 15 min at 37 °C with Restore™ Western Blot Stripping Buffer (ThermoFisher scientific) to remove the anti-C3 primary antibody. Then the membranes were incubated with rabbit anti-C4d (0.2 μg/mL; Hycult) followed by anti-rabbit peroxidase-conjugated antibodies (0.16 μg/mL, Santa Cruz Biotechnology). Immunocomplexes were visualized by chemiluminescence using the IMMOBILON western blot substrate (Merck KGaA). Quantifications were done with Image Lab Software (Bio-Rad) and results were standardized using the total protein loaded (Ponceau solution, Bio-Rad). Complete gels are shown in Supplementary Fig. S3.

2.15. Experimental design and statistics

Mice were randomly allocated to surgery and assigned across cages and days. To minimize variability, all surgeries were done by the same investigator. Subsequent behavioral, histological and biochemical evaluations were done by blinded investigators. Groups were compared by analysis of variance and post hoc test, as indicated in each figure legend. The parametric or non-parametric test was selected after a Kolmogorov-Smirnov test or a Shapiro-Wilk test (for small-sized groups) for normality to assess whether groups met normal distribution. The constancy of variances was checked by Bartlett test and, if not satisfied, a Welch correction was used. Group size for testing the efficacy of pd- or rhC1INH treatment at 48 h after tMCAo was defined pre hoc using the formula: $n = 2\sigma^2 f(\alpha, \beta)/\Delta^2$ (SD in groups = σ, type 1 error $\alpha = 0.05$, type II error $\beta = 0.2$, percentage difference between groups $\Delta = 30$). For each measure, the standard deviation (SD) between groups was calculated on the basis of the composite neuroscore, set as the primary outcome, measured on wild type (WT) mice in previous experiments using the same model ($\sigma = 23$, yielding $n = 9.29$). To limit the use of animals, a post hoc power analysis test was done at $n = 6$ on raw data for each experimental branch. The experiment was interrupted at $n = 6$ since: 1) rhC1INH treatment showed significant protection; 2) pdC1INH treatment was unable to provide significant differences using a reasonable number of animals ($\Delta = 4.5$, $\sigma = 23.48$, thus expected $n = 432.90$). A "health score" was obtained stratifying neuroscore, ischemic volume and neuronal count datasets on WT mice into four groups according to their quartiles, as previously published (Neglia et al., 2020b). To each quartile a score ranging from 4 (good outcome) to 1 (bad outcome) was attributed. The total score was the sum of the body weighted scores of the three parameters, e.g. neuroscore accounted for 50%, ischemic volume for 25% and neuronal count for 25% (striatum and cortex for 12.5% each) of the final score. A good outcome was defined as a score >3, while a poor outcome as score <2. Statistical analysis was done using GraphPad Prism (GraphPad Software Inc., San Diego, CA, USA, version 7.0); p values lower than 0.05 were considered significant.

3. Results

To evaluate sensorimotor deficits, mice were rated according to neuroscore at 48 h after tMCAo. As shown in Fig. 1A, mice treated with rhC1INH showed significantly lower deficits than those treated with vehicle (17.7 ± 3.9 vs. 26.0 ± 4.6, mean ± sd of composite neuroscore, p

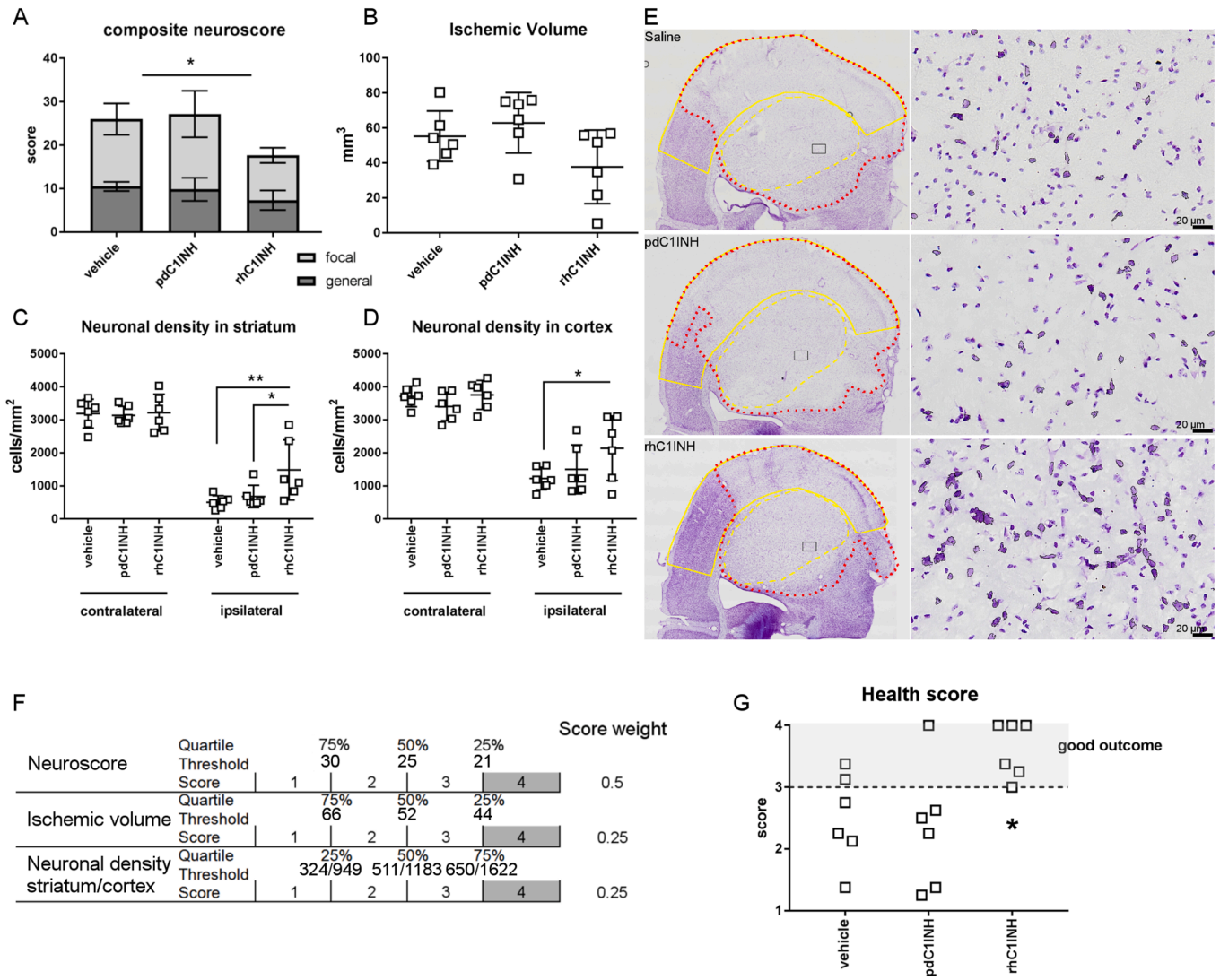

Fig. 1. Ischemic outcome at 48 h after tMCAo in mice treated with pdC1INH or rhC1INH. A) Composite neuroscore outcome. Mice treated with rhC1INH showed amelioration of sensori-motor deficits. These beneficial effects were not shown in mice treated with pdC1INH. Data shown as bars, mean ± sd, n = 6. One-way ANOVA followed by Dunnett's test, *p < 0.05 vs. vehicle. B) Quantification of the ischemic volume. Data shown as scatter dot plot, line at mean ± sd, n = 6. One-way ANOVA followed by Dunnett's test, not significant but with a decreased trend in ischemic volume for rhC1INH-treated mice. C) Quantification of survived neurons in striatum. Mice treated with rhC1INH had higher neuronal density than vehicle or pdC1INH-treated mice in the ipsilateral striatum. Data expressed as neurons/mm^2 and shown as scatter dot plot, line at mean ± sd, n = 6. Two-way ANOVA followed by Tukey's multiple comparison test, *p < 0.05, **p < 0.01. D) Quantification of survived neurons in cortex. Mice treated with rhC1INH had more neuronal density than vehicle-treated mice in the ipsilateral cortex. Data expressed as neurons/mm^2 and shown as scatter dot plot, line at mean ± sd, n = 6. Two-way ANOVA followed by Tukey's multiple comparison test, *p < 0.05. E) Representative microphotographs of Cresyl violet stained brain sections. Left) the extent of the ischemic lesion (red dotted outline) appeared smaller in rhC1INH-treated mice than vehicle or pdC1INH-treated mice. The quantification of neuronal density was done in striatum (yellow dotted outline) or in cortex (yellow solid outline). Right) high magnifications of the insert in striatum showing the quantified neurons, corresponding to cells sized over the cut-off at 25 μm^2. Scale bar 20 μm. F) A health score was defined based on quartiles distributions of the neuroscore, ischemic volume and neuronal density, with cut-offs relative to vehicle-treated mice. G) Health score outcome. Mice having a health score > 3, considered like those with a good outcome, appeared more frequently after rhC1INH than after vehicle or pdC1INH treatment. Data shown as dot plots, n = 6. One-way ANOVA followed by Dunnett's test, *p < 0.05 vs. vehicle. (For interpretation of the references to colour in this figure legend, the reader is referred to the web version of this article.)

< 0.05) while mice receiving pdC1INH were not protected (27.17 ± 7.7). Furthermore, the protective effect of rhC1INH was observed also when stratifying the composite neuroscore according to general and focal deficits (7.3 ± 2.3 vs. 10.5 ± 1.0 and 10.33 ± 1.8 vs. 15.5 ± 3.6, rhC1INH vs vehicle controls, respectively).

We next measured the lesion extent using a histological analysis on Cresyl violet stained sections. Mice treated with rhC1INH showed a 32% decrease of ischemic volume compared to vehicle (37.74 ± 21.02 vs. 55.24 ± 14.48, mean ± sd of mm^3, p = 0.18). Mice treated with pdC1INH had a lesion volume of 62.89 ± 17.31 mm^3 (Fig. 1B). When analyzing the number of survived neurons in the ischemic striatum, mice treated with rhC1INH had significantly higher neuronal density in the ipsilateral region compared to vehicle (1484 ± 909.6 vs. 508 ± 199.0 neurons/mm^2) or to pdC1INH-treated mice (681 ± 338.9 neurons/mm^2, Fig. 1C). In ipsilateral cortex, mice treated with rhC1INH had higher neuronal density than vehicle-treated (2141 ± 977 vs. 1225 ± 340, Fig. 1D). No difference of neuronal density in the reference, non-ischemic contralateral region was observed. Microphotographs displayed in Fig. 1E show typical Cresyl violet staining for each experimental condition. The volume of the ischemic lesion was obtained outlining the pale area corresponding to the ischemic region (red dotted outline, left panels). Within the ischemic areas, after having traced

regions of interest in the striatum (yellow dotted outline) or cortex (yellow solid outline), the number of survived neurons was calculated by digital image analysis to segmentate neurons (right panels). Cresyl violet positive neurons were distinguished from glial cells based on their size, by applying a cell area cut-off of 25 μm^2 (Supplementary Fig. S1). We further assessed the presence of apoptotic cells in striatum and cortex finding no differences among the three experimental groups (Supplementary Fig. S4 and S5). We also quantified the number of apoptotic hippocampal neurons, finding a non-significant trend towards decreased apoptosis after rhC1INH treatment compared to vehicle (211 ± 287 vs. 440 ± 290, mean ± sd of cell density per mm^2, $p = 0.35$ after one-way ANOVA followed by Dunnett's multiple comparisons, supplementary Fig. S6).

In order to evaluate the degree of protection of treatment with rhC1INH or pdC1INH, we calculated a health score taking into account both the behavioral and the histological measures as previously published (Neglia et al., 2020b) (Fig. 1F). The result showed that mice receiving rhC1INH were more likely to develop a good outcome, defined as a cut-off health score >3, than vehicle- or pdC1INH-treated mice (Fig. 1G).

We then analyzed the concentration C1INHs in mouse plasma at two time points after tMCAo, namely 90 min and 48 h (corresponding to 30 min and 47 h post C1INH dose), comparing vehicle, pd- and rhC1INH-treated mice. For this, we developed a method using surface plasmon

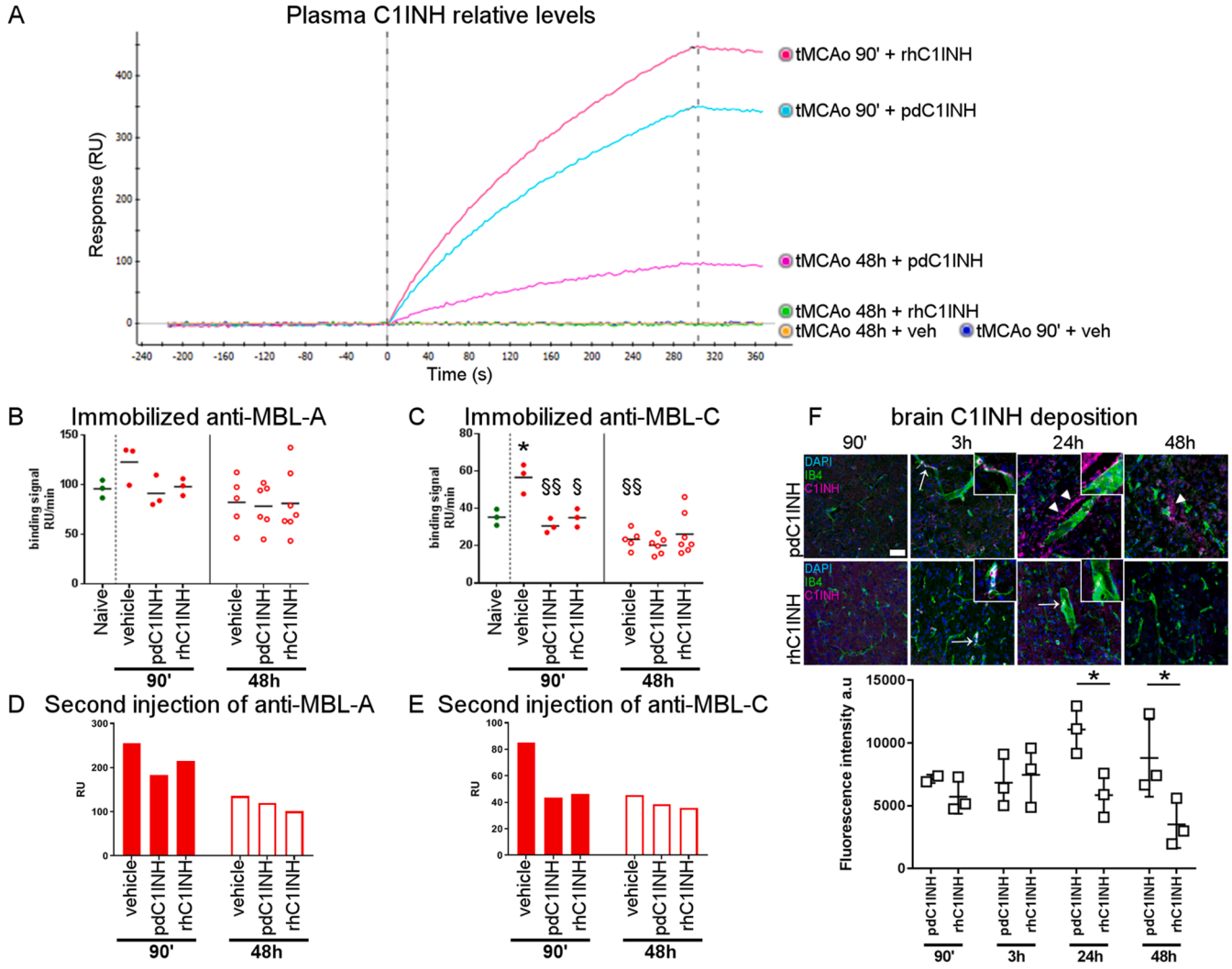

Fig. 2. Surface plasmon resonance studies and C1INH brain presence at different times after tMCAo. A) Presence of human C1INH in the plasma of treated mice, as detected by SPR. A polyclonal antibody against human C1INH was immobilized on the sensorchip. Then plasma from tMCAo mice were injected. Then the polyclonal anti-human C1INH antibody was injected to amplify the signal and the figure shows the corresponding sensorgrams. At 90 min after tMCAo (i.e. 30 min after treatment) both pd- and rhC1INH were detected in plasma, while at 48 h (i.e. 47 h post dose) only pdC1INH signal was found. Plasma from vehicle-treated mice did not show any signal. B, C) SPR specific binding signals obtained upon injection of plasma samples from naive mice or mice at 90 min or 48 h after tMCAo (30 min or 47 h after treatment, respectively) on SPR sensor surfaces coated with immobilized anti-MBL-A antibody (B) or immobilized anti-MBL-C antibody (C). Data are expressed as binding signals (RU/min) and shown as scatter dot plot, line at mean, n = 3–6. Two-way ANOVA followed by Sidak's multiple comparison test, *$p < 0.05$ vs. naive, §$p < 0.05$; §§$p < 0.01$ vs tMCAo 90 min (i.e. 30 min after treatment) + vehicle. D, E) Pools of plasma belonging to the same experimental conditions were injected on a sensorchip coated with immobilized anti-MBL isoforms antibodies, followed by a second injection of anti-MBL-A (D) or anti-MBL-C (E) to amplify the signal. The results confirmed those presented in B and C. F) Representative extended-focus microphotograms of brains labeled for C1INH (purple), vessels (IB4, green) and nuclei (DAPI). Arrows indicate vascular C1INH, arrowheads extravasated C1INH. Scale bar 40 μm. Quantification by immunofluorescence of C1INH presence in brain. Both pd- and rhC1INH were present and quantifiable starting at 90 min after tMCAo (i.e. 30 min after treatment). pdC1INH peaked at 24 h and was higher than rhC1INH at 24 h and 48 h after tMCAo (i.e. 23 h and 47 h after treatment, respectively). Data shown as scatter dot plot, line at mean, n = 3. Two-way ANOVA (treatment effect $p = 0.005$) followed by Sidak's multiple comparison test, *$p < 0.05$. (For interpretation of the references to colour in this figure legend, the reader is referred to the web version of this article.)

resonance (SPR). We immobilized polyclonal anti-hC1INH antibody or control IgG on parallel surfaces of the same sensorchip and flowed mouse plasma on them. Then, we injected again the same polyclonal anti-C1INH antibody, achieving signal amplification compared to that obtained after plasma injection (Supplementary Fig. S2 and S3). The SPR signal, proportional to circulating hC1INH concentrations, showed that both pd- and rhC1INH were present in plasma at 90 min after tMCAo, but only pdC1INH was still detectable at 48 h after tMCAo (Fig. 2A). These data are in line with those observed in humans, indicating a shorter plasma half-life of rhC1INH in comparison to pdC1INH. No signal was obtained in plasma from vehicle-treated mice, at either time points, thus demonstrating that the anti-hC1INH used was specific to the injected human C1INH (of human origin) and could not detect endogenous C1INH.

Plasma samples from naive or ischemic mice were also injected on sensorchips coated with anti-MBL-A or anti-MBL-C antibodies. Sensor surfaces coated with BSA were used as reference. For each plasma sample, the signals obtained on BSA were subtracted in order to obtain the specific MBL-dependent signals, which are shown in Fig. 2B and C. Comparison with vehicle-treated mice indicate that tMCAo increased MBL-A and MBL-C dependent signals, as early as 90 min after the ischemic onset, returning to basal levels after 48 h. An increase of SPR signals can be due to increased levels of circulating MBL or to higher mass of binding species, i.e. that MBL active complexes might form or increase upon ischemia. Treatment with pd- and rhC1INH at reperfusion, counteracted the tMCAo-induced increase of MBL-A and MBL-C dependent signals, with the signal of MBL-C changed in statistically significant manner (Fig. 2C). These SPR results were confirmed when the experiment was repeated on plasma pools using the sandwich design with immobilized and injected anti-MBL-A or anti-MBL-C antibodies to have amplified signals (Fig. 2D, E).

We next analyzed the brain presence of C1INHs using quantitative immunofluorescence, at different times after tMCAo. The antibody used to label C1INHs was not able to detect mouse endogenous C1INH, since the fluorescent signal was absent in vehicle-treated mice. Brain C1INH presence was similar at 90 min and 3 h after tMCAo (corresponding to 30 min and 2 h post C1INH dose) in pd- or rhC1INH-treated mice (respectively, 7148 ± 333 vs. 5734 ± 1368 and 6848 ± 2080 vs. 7469 ± 2389 fluorescence arbitrary units). At variance with these time points, mice receiving rhC1INH had lower brain presence of C1INH than pdC1INH-treated at 24 h (11084 ± 1886 vs. 5856 ± 1742, 23 h post C1INH dose) and 48 h (8806 ± 3075 vs 3522 ± 1879, 47 h post C1INH dose) after tMCAo (Fig. 2F).

In order to assess brain local inflammation, we measured brain myeloid cell activation using CD11b labeling. We analyzed ischemic mice at 48 h after tMCAo, and did not find statistically significant differences among experimental groups when measuring total CD11b stained area (Fig. 3A), CD11b circularity (index of ameboid reactive transformation, Fig. 3B) and CD11b grid touchings (index of ramification density, Fig. 3C).

MBL deposition on ischemic vessels is a hallmark of lectin pathway activation in ischemic stroke, and is critically associated with vascular dysfunction and lesion expansion (Orsini et al., 2018). At 48 h after tMCAo, the murine MBL-C isoform is most prominently seen in this model as reported previously (Neglia et al., 2020b). We therefore analyzed MBL-C by quantitative immunofluorescence and observed significantly less deposition of MBL-C in rhC1INH-treated mice (373 ± 378 pixel integrated density/1000) compared to vehicle or pdC1INH-treated mice (1106 ± 517 or 1236 ± 480, respectively. Fig. 3D, E). C1INH and MBL-C were found to co-localize on the ischemic vessels of rhC1INH-treated mice at both 90′ and 48 h after tMCAo (Fig. 3F).

Deposited MBL was reported to affect small vessel hemodynamics in the ischemic territory after the initial event (Orsini et al., 2018) by different mechanisms, including the promotion of fibrin deposition (de la Rosa et al., 2014). We here analyzed the presence of fibrin in the cortical ischemic territory by immunofluorescence, using an antibody that was not able to distinguish it from its precursor fibrinogen. We observed lower fibrin(ogen) deposition in rhC1INH-treated compared to vehicle-treated mice (0.21 ± 0.19 vs. 0.54 ± 0.17 mean ± sd of area fraction, $p = 0.033$ Fig. 3G, H).

On MBL binding to its target, the lectin pathway of complement is activated, resulting in the formation of cleaved products of C4 and C3. We performed Western blot analysis of C3b (110 kDa) and C4b (75 kDa) active fragments in plasma from vehicle, pd- or rhC1INH-treated mice at 48 h after tMCAo (Fig. 4A, the complete gel is shown as Supplementary Fig. S7). C3b formation was non-significantly reduced in plasma from rhC1INH-treated mice (Fig. 4B). C4b formation decreased significantly in plasma after rhC1INH ($4.5 \cdot 10^{-4} \pm 3.1 \cdot 10^{-4}$ mean ± sd of C4b OD/total protein OD) compared to vehicle ($12.6 \cdot 10^{-4} \pm 1.8 \cdot 10^{-4}$) or pdC1INH ($10.1 \cdot 10^{-4} \pm 4.9 \cdot 10^{-4}$) treatment (Fig. 4C). We also analyzed the plasma presence of thrombomodulin lectin-like domain 1 (TMD1) – a 25 kDa cleavage product of the membrane-bound protein thrombomodulin with anti-complement and anti-thrombotic properties. No differences in its plasma presence were seen among experimental groups (Fig. 4D).

In order to assess the contribution of endogenous C1INH to ischemic injury responses, we developed C1INH knock-out mice using the CRISPR-Cas9 technology. C1INH KO mice were subjected to tMCAo and were treated or not with rhC1INH at reperfusion. To rule out possible differences in the brain vascular architecture affecting the ischemic outcome, we compared the vascular anatomy of C1INH KO mice with that of the wild types used as controls (C57BL/6N). We traced the anastomotic line between the MCA and anterior carotid artery and calculated its distance from the brain midline in correspondence with positions at 4 and 6 mm from the frontal pole (Fig. 5A), as published elsewhere (Orsini et al., 2016; Perego et al., 2019). We could not detect significant differences of cerebral vascular anatomy in C1INH KO mice (Fig. 5B).

At 48 h after tMCAo, C1INH KO displayed a non-significant trend towards higher behavioral deficits (Fig. 5C, deficits were 23.9 ± 8.0 mean ± sd) and lesion (Fig. 5D, ischemic volume was 58.2 ± 12.1 mean ± sd of mm^3) compared to WT (18.9 ± 7.8 deficits and 44.1 ± 12.1 mm^3) or rhC1INH-treated C1INH KO mice (20.6 ± 7.7 deficits and 45.9 ± 21.9 mm^3). Neuronal density in C1INH KO mice was lower in the striatum (670 ± 215 neurons/mm^2, Fig. 5E) and the cortex (1142 ± 453, Fig. 5E') compared to WT mice (900 ± 322 and 1869 ± 1089, respectively). The treatment of C1INH KO mice with rhC1INH partially reduced the neuronal loss, with these mice having similar neuronal density in the striatum (1290 ± 1139) and the cortex (2073 ± 1251) as WT mice. We point out that C1INH KO mice were compared to C57BL/6N WT in order to match their background strain. We observed that C57BL/6N mice developed less severe injury after tMCAo (lower sensorimotor deficits and lower tissue damage) than C57BL/6J, the strain used to compare the C1INH treatments in this work (see Fig. 1 for reference). This is in line with the observation that the susceptibility to MCAo may vary across mouse strains (Du et al., 2015).

The measure of the health score combining behavioral and histological data (Fig. 5G) showed that C1INH KO mice were more likely to develop a poor outcome (score cut–off < 2) than WT mice or rhC1INH-treated C1INH KO mice, which was statistically significant (Fig. 5H). MBL-C vascular deposition in the ischemic territory did not vary among experimental groups (Fig. 5I, J).

4. Discussion

The present study identifies MBL as a key target of rhC1INH in an *in vivo* model of ischemia/reperfusion injury. We report the neuroprotective effects of rhC1INH administered as a single dose at 15 U/mouse (mean dose 561 U/kg) by systemic injection at reperfusion in a murine model of severe ischemic stroke induced by 60 min MCAo. In contrast, the administration of pdC1INH using the same protocol and dose (units/mouse) did not provide neuroprotection. This latter

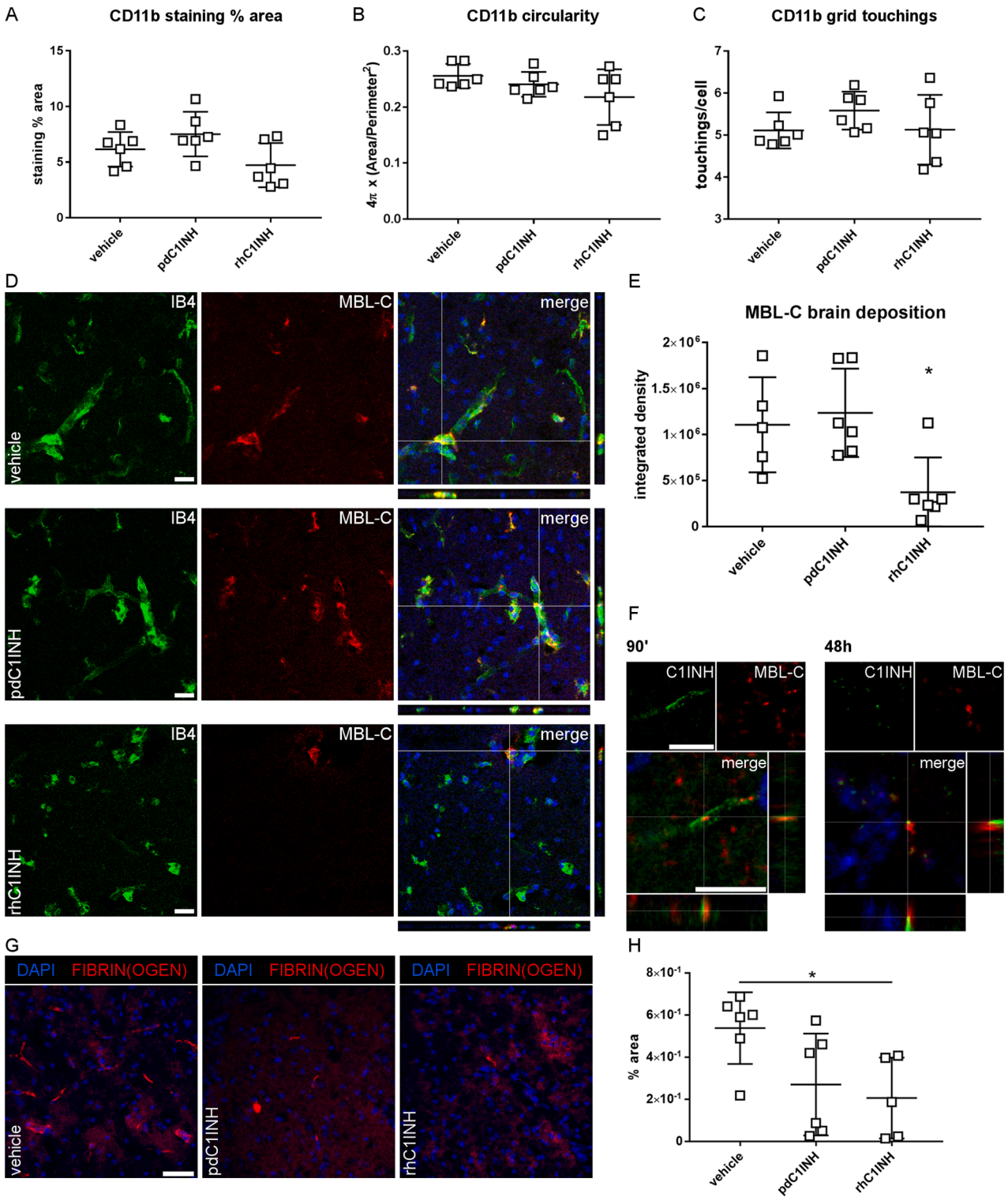

Fig. 3. Local brain inflammatory response in ischemic mice at 48 h after tMCAo. A) Microglia/macrophage reactivity was analyzed after CD11b immunostaining. No difference in total stained area was observed. Data shown as scatter dot plot, line at mean ± sd, n = 6. One-way ANOVA followed by Dunnett's test, not significant. B) CD11b cell circularity did not change on treatment. Data shown as scatter dot plot, line at mean ± sd, n = 6. One-way ANOVA followed by Dunnett's test, not significant. C) CD11b cell ramifications, calculated as the mean number of touchings on a superimposed 9x9 μm grid, did not change. Data shown as scatter dot plot, line at mean ± sd, n = 6. One-way ANOVA followed by Dunnett's test, not significant. D) Representative images showing MBL-C (red) deposition on ischemic vessel (IB4, green; delineating the investigated blood vessels) by immunofluorescence. Scale bar 20 μm. E) MBL-C signal quantification within the vessels showed lower MBL-C presence in mice treated by rhC1INH compared to vehicle or pdC1INH-treated mice. Data shown as scatter dot plot, line at mean ± sd, n = 5–6. One-way ANOVA followed by Dunnett's test, *$p < 0.05$ vs. vehicle and pdC1INH. F) Confocal analysis showing C1INH (green) co-localizing with MBL-C (red) at 90′ and 48 h after tMCAo in rhC1INH-treated mice. Nuclei are in blue. Scale bar 20 μm. G) Representative microphotographs of fibrin(ogen) immunofluorescence (red) in the ischemic cortex. Scale bar 40 μm. H) Fibrin(ogen) presence was lower in mice treated by rhC1INH compared to vehicle. Data shown as scatter dot plot, line at mean ± sd, n = 5–6. One-way ANOVA followed by Dunnett's test, *$p < 0.05$ vs. vehicle. (For interpretation of the references to colour in this figure legend, the reader is referred to the web version of this article.)

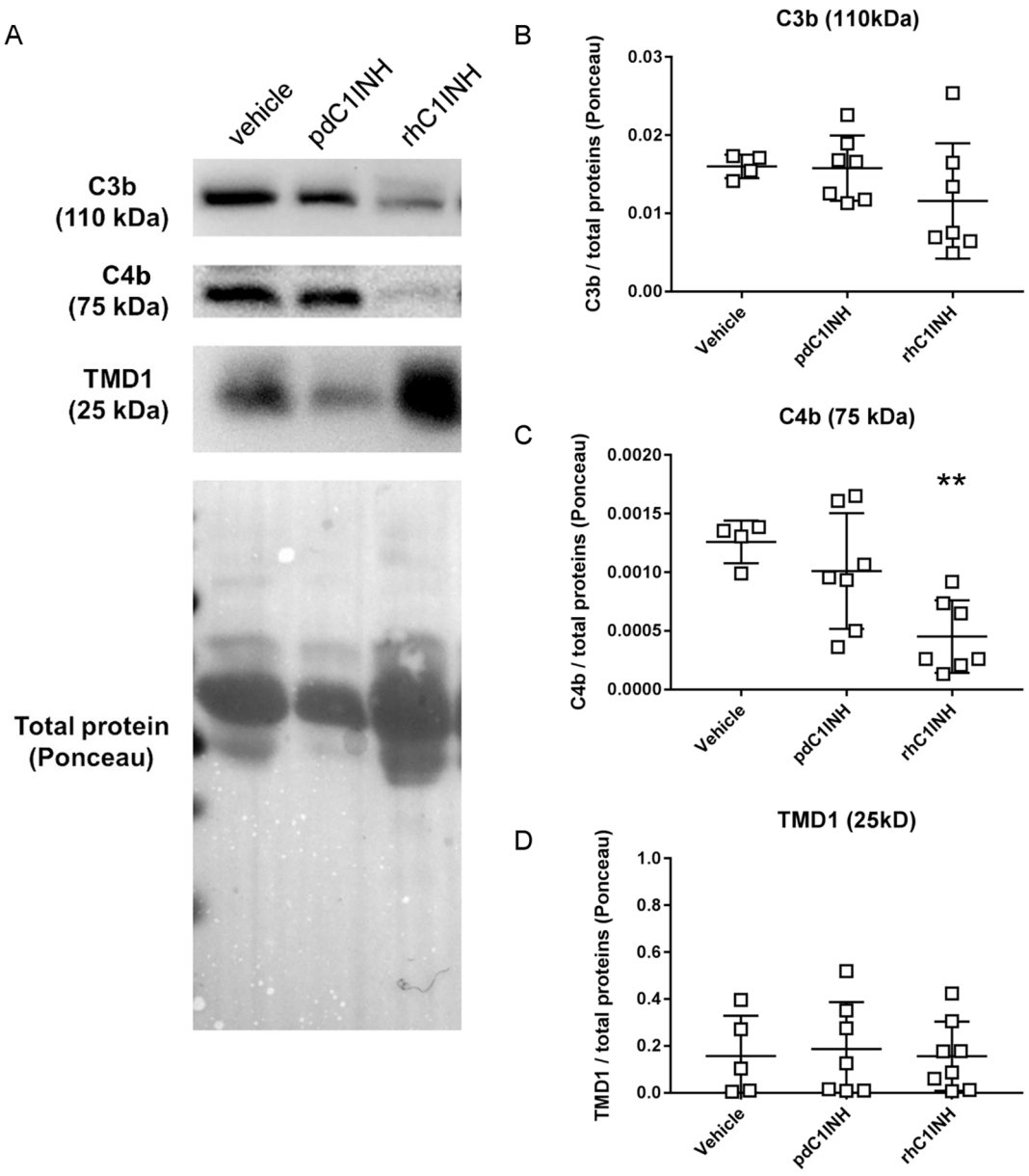

Fig. 4. Plasma levels of C3b, C4b and TMD1 at 48 h after tMCAo. A) Western blot showing bands relative to C3b fragments (110 kDa), C4b fragments (75 kDa) and thrombomodulin lectin-like domain 1 (TMD1, 25 kDa). Total proteins in plasma were labeled by Ponceau Red and served for normalization for band densitometric quantification. B) The quantification of plasma C3b fragments, although showing a tendency in lower levels in rhC1INH-treated mice compared to vehicle or pdC1INH-treated mice, did not resulted in significant differences. C) Plasma C4b was lower in rhC1INH compared to vehicle or pdC1INH-treated mice. D) Plasma TMD1 did not vary upon treatments. Data shown as scatter dot plot, line at mean ± sd, n = 4–7. One-way ANOVA followed by Dunnett's test, $^{**}p < 0.01$ vs. vehicle.

observation differed compared to previous studies reporting the efficacy of plasma derived C1INH in similar models of ischemia/reperfusion injury (Chen et al., 2018; Heydenreich et al., 2012). Specific differences among the studies are the injury severity and the time point for outcome assessments, partially explaining the different observations on pdC1INH efficacy and posing a rationale for future multicentric pre-clinical studies. Notably, all studies concluded that the protective effects of C1INHs were associated with decreased complement activation and dampening of thrombotic mechanisms.

Exploring the mechanism by which rhC1INH was more effective in our animal model of stroke than pdC1INH, the findings demonstrate that rhC1INH more potently reduced the activation of the lectin pathway of complement, possibly through MBL binding and consequent inhibition.

MBL is one of the recognition molecules of the lectin pathway, whose central role in the pathophysiology of brain ischemic injury was reported in experimental models and patients (Cervera et al., 2010; Fumagalli and De Simoni, 2016; Osthoff et al., 2011; Song et al., 2015; Zhang et al., 2015). Previous data by our group and others demonstrated that, besides the activation of the complement system, MBL controls different vascular events contributing to ischemic lesion expansion. In fact, MBL is implicated in platelet activation and IL-1α release (Orsini et al., 2018), in the formation of deposits of fibrin in the ischemic vessels (de la Rosa et al., 2014), and in endothelial cell damage (Neglia et al., 2020a). Being at the crossroads of different blood-borne cascades after stroke, MBL represents a promising pharmacological target. Moreover its druggability in the context of acute brain injury was demonstrated using intravenously administered compounds, that do not need to cross the blood brain barrier (BBB) to reach the target (De Blasio et al., 2017; Orsini et al., 2012). This latter point is crucial, as BBB crossing stands as a major limitation for many anti-inflammatory molecules that failed clinical transferability for stroke treatment.

Among the compounds targeting MBL, rhC1INH provided promising

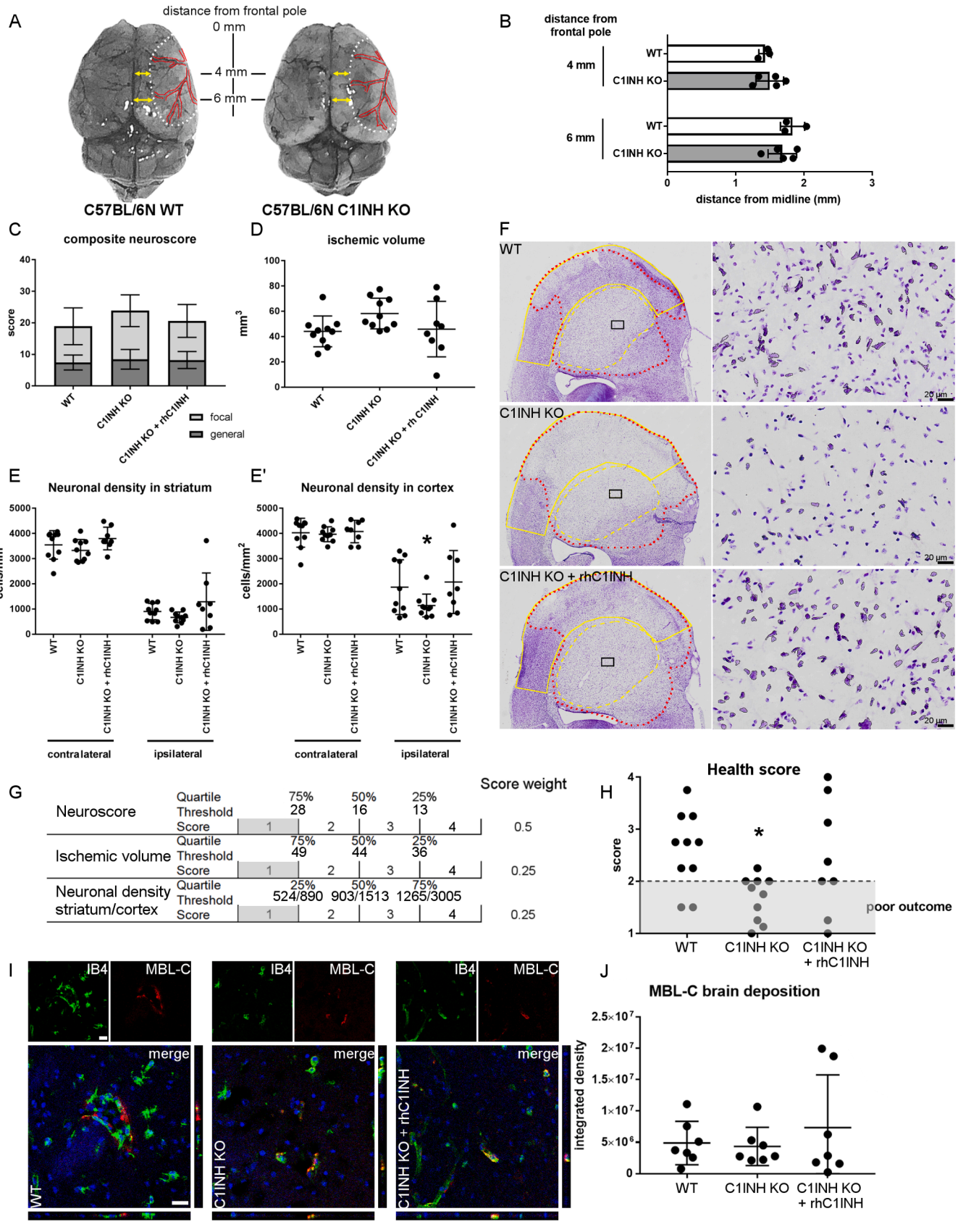

(caption on next page)

Fig. 5. Ischemic outcome at 48 h after tMCAo in WT vs. C1INH KO mice, treated or not with rhC1INH. A) Anastomotic line (yellow) connecting the terminal branches of the middle. cerebral artery and the anterior cerebral artery of wild-type (WT) and C1INH KO mice. B) Distance (millimeters) of the anastomotic line to the midline at 4 and 6 mm from the frontal pole in the brains of WT and C1INH KO mice. Data shown as bars, mean ± sd, n = 3–5. Two-way ANOVA followed by Sidak's multiple comparisons, not significant. C) Sensori-motor deficits did not differ comparing the different conditions. Data shown as bars, mean ± sd, n = 13. One-way ANOVA followed by Dunnett's test, not significant. D) Quantification of the ischemic volume showed a trend towards increased lesion size in C1INH KO mice, not observed after rhC1INH administration at reperfusion. Data shown as scatter dot plot, line at mean ± sd, n = 8–10. One-way ANOVA followed by Dunnett's test, not significant. Quantification of survived neurons in E) striatum and E') cortex showed decreased neuronal density in cortex of C1INH KO mice. Data expressed as neurons/mm^2 and shown as scatter dot plot, line at mean ± sd, n = 8–10. Two-way ANOVA followed by Tukey's multiple comparison test, *p < 0.05 vs. C1INH KO + rhC1INH. F) Representative microphotographs of Cresyl violet stained brain sections. Left) the extent of the ischemic lesion (red dotted outline) appeared smaller in WT than C1INH KO mice. The quantification of neuronal density was done in striatum (yellow dotted outline) or in cortex (yellow solid outline). Right) high magnifications of the insert in striatum showing the quantified neurons, corresponding to cells sized over the cut-off at 25 μm^2. Scale bar 20 μm. G) A health score was defined based on quartiles distributions of the neuroscore, ischemic volume and neuronal density, with cut-offs relative to WT mice. H) Mice having a health score <2, considered like those with a poor outcome, appeared more frequently in C1INH KO than WT or C1INH KO treated with rhC1INH. Data shown as dot plots, n = 8–10. Welch ANOVA test followed by Dunnett's T3 multiple comparison test, *p < 0.05 vs. WT. I) Representative images showing MBL-C (red) deposition on ischemic vessel (IB4, green; delineating the investigated blood vessels) by immunofluorescence. Scale bar 20 μm. J) MBL-C signal quantification within the vessels showed no variation across experimental groups. Data shown as scatter dot plot, line at mean ± sd, n = 6. Welch ANOVA followed by Dunnett's T3 multiple comparison test, not significant. (For interpretation of the references to colour in this figure legend, the reader is referred to the web version of this article.)

results in experimental models. C1INH is an endogenous inhibitor of complement system proteases, belonging to the serpin superfamily. C1INH inhibits the lectin pathway inhibiting the MBL-associated serine protease (MASPs) that start the proteolytic cascade of complement activation. Moreover C1INH plays a central role in the cross-talk among the complement, coagulation, fibrinolytic and kallikrein-kinin systems (Landsem et al., 2016), all involved in modulation of endothelial function (Wu et al., 2020).

C1INH is used clinically as a plasma-derived or recombinant human product for the treatment of HAE, a rare disease due to partial C1INH deficiency characterized by episodes of severe swellings. Recombinant human C1 inhibitor (rhC1INH) is approved for the treatment of acute angioedema attacks in HAE patients. RhC1INH has the same amino acid sequence as human endogenous C1INH, but it has a different glycosylation profile, which results in a shorter plasma half-life. Pharmacokinetic evaluation using SPR with antibody-mediated amplification of the signal confirmed that both pd- and rhC1INH were seen abundantly present 90 min after the ischemic onset (i.e. 30 min after administration, at reperfusion), but only pdC1INH was still present at 48 h after tMCAo. Nonetheless, rhC1INH- but not pdC1INH-treated mice were protected from ischemic injury when behavioral and histological outcomes were analyzed at 48 h, suggesting that the presence of rhC1INH early in the post-ischemic period is particularly protective. Specifically, the behavioural neuroscore showed lower general and focal deficits with rhC1INH-treated mice compared to pdC1INH and vehicle-treated mice. Additionally, a lower ischemic volume and a higher number of survived neurons were observed in rhC1INH-treated mice compared to pdC1INH- and vehicle-treated mice. Thus, rhC1INH exerted a protective effect after ischemia/reperfusion injury independently of its short half-life.

We then focused on MBL as a target of C1INH and aimed at assessing if C1INH products targeted it differently. Using SPR we measured MBL mouse circulating isoforms (MBL-A and MBL-C) in healthy (naive) or ischemic mice, by coating the SPR sensorchip with monoclonal anti-mouse MBL isoforms antibodies. Both isoforms showed increased signal in vehicle-treated tMCAo mice at 90 min compared to naïve. The observed SPR signal increase can be due to increased levels of circulating MBL or to higher mass of binding species related to MBL active complexes. MBL isoform circulating levels were reported to decrease acutely after experimental ischemia, an event due to consumption as a result of target binding (Neglia et al., 2020b). Increased SPR signal thus suggests MBL oligomerization in response to ischemia, in line with the hypothesis that MBL multimeric organization favors the recognition of spatially distinct regions on its target (i.e. activated endothelium), which provides high avidity (Sheriff et al., 1994). The fact that SPR signal amplification was achieved flowing the same monoclonal anti-MBL isoform antibodies suggested the presence of oligomeric MBL complexes, since the immobilized anti-MBL antibodies could not saturate all the specific epitopes. When pd or rhC1INH were present, MBL mass did not increase 90 min after tMCAo, thus implying that either treatments interfered with MBL's multimeric assembly – and possibly functioning – early after the ischemic onset. The effect was more pronounced for the MBL-C than the MBL-A isoform.

We then moved to the analysis of the presence of C1INH products and MBL-C in the brain ischemic region. Both C1INH products were present in the brain starting from 90 min after ischemia. At 24 h and 48 h after ischemia, pdC1INH was present at a higher amount compared to rhC1INH. This observation mirrors the plasma concentrations of the two C1INHs. It cannot be excluded however that reacted rhC1INH, not detected by immunofluorescence, resulted in underestimation of rhC1INH concentration measured in the brain.

According to the immunostaining images, pdC1INH appeared to leak into the brain parenchyma, a less frequent occurrence for rhC1INH. This observation is in line with a previous one obtained following the 30 min tMCAo model (Gesuete et al., 2009), and possibly implies a more selective targeting of deposited MBL by rhC1INH. Indeed, MBL is mainly present intravascularly at the considered time points, showing limited extravasation due to its molecular size. Measuring MBL-C brain presence at 48 h after tMCAo – a time when this murine isoform is mostly seen (Neglia et al., 2020b) – we show that it was decreased following rhC1INH treatment. Confocal images showed a direct interaction between rhC1INH and MBL-C on the ischemic vessels. In line with the direct targeting of MBL, the formation of complement C4b active fragments – hallmark of complement activation – was lower in rhC1INH- compared to pdC1INH-treated mice at 48 h after tMCAo. The formation of complement C3b fragments was only slightly decreased by rhC1INH treatment, possibly indicating that other complement pathways, i.e. the classical and the alternative, were still active. The protective effects of rhC1INH at 48 h after tMCAo seemed to depend on the modulation of vascular responses, since local brain inflammation, i.e. microglia activation, did not differ with the treatment. In line with rhC1INH modulation of vascular responses, we observed lower presence of fibrin deposits in the ischemic territory of mice receiving it. Fibrin deposits are associated with secondary thrombotic mechanisms after stroke. Moreover MBL presence was associated with the formation of fibrin deposits, as part of its deleterious effects in a model of experimental stroke (de la Rosa et al., 2014). As such rhC1INH, by targeting MBL, could dampen secondary thromboinflammatory events that follow ischemia/reperfusion injury. The different pharmacokinetic profile of the inhibitors may contribute to their different efficacy. It is possible that MBL and its downstream mechanisms are deleterious in the hyperacute stages of stroke, but beneficial at later stages, i.e. by facilitating efferocytosis and brain remodelling.

In order to prove the importance of C1INH in the context of brain ischemia, we developed mice deficient for C1INH and subjected them to tMCAo. C1INH KO mice had a worse ischemic outcome at 48 h after tMCAo than WT, as indicated by the health score combining behavioral

and histological assessment of the lesion. A single dose of rhC1INH at reperfusion could improve the outcome of C1INH KO mice, making them not different from WT. Thus, C1INH has a central role in post-stroke inflammatory events, being an endogenous suppressor of inflammatory events that lead to injury expansion. The fact that a single dose of rhC1INH at reperfusion partially reverted the outcome in C1INH KO mice lends support to complement's early activation after injury. In line with this, we observed the formation of MBL complexes as early as 90 min after the ischemic onset in WT mice. However, since a single dose of rhC1INH did not improve the outcome of C1INH KO compared to untreated WT, we hypothesize that C1INH's suppressive functions continue over a period exceeding rhC1INH's plasma residence time. Indeed, rhC1INH proved a wide window of efficacy when administered up to 18 h after 30 min tMCAo (Gesuete et al., 2009), using a milder model of ischemia/reperfusion than that used here. Future studies should explore the time window of efficacy of rhC1INH after 60 min tMCAo, a model associated with stronger inflammatory events than 30 min tMCAo (Denes et al., 2007; Zhou et al., 2013). Differences in rhC1INH neuroprotective properties depending on stroke severity and types are indeed foreseen, since when we administered rhC1INH to mice subjected to permanent ischemia, its time window of efficacy, defined as the time between ischemia and administration of rhC1INH, was 6 h (Gesuete et al., 2009). Understanding rhC1INH's behavior in different stroke types is a critical piece of information, considering the importance of a wide therapeutic window for stroke patients. Moreover unwanted interactions of exogenously administered C1INH with tPA – used for the thrombolytic therapy in stroke patients – have been reported (Pannell et al., 2015; Tomasi et al., 2011). Thus, in the clinical scenario, it could be hypothesized that rhC1INH administration could follow that of tPA, a drug given within 4.5 h after stroke and characterized by a rapid clearance. Alternatively, rhC1INH could be used in those cases for which tPA is not recommended, i.e. in patients presenting for treatment after tPA's therapeutic window.

In conclusion, our study provides insights on rhC1INH targets and anti-inflammatory effects in experimental ischemia/reperfusion injury. rhC1INH places as a promising drug for the treatment of severe stroke. We acknowledge some limitations of the present study, such as the treatment done only at reperfusion and the use of young male mice for the ischemic model. Thus open questions regard rhC1INH's time window of efficacy in this model of stroke, the best treatment protocol – i.e. single vs. multiple dosing – and the safety and efficacy in combination with comorbidities and with the pharmacological interventions that currently are part of the standard of care for stroke.

Funding

The execution of the study was supported by Pharming Technologies B.V. Pharming Technologies B.V. contributed in study design, the interpretation of data and in the writing of the manuscript.

Author contribution

DM, AP, AV and MO performed the experiments and analyzed the data, YP and EVA conceived the work and discussed the data and coordinated technical analysis on the compounds used, MGDS and MG conceived the work, analyzed and discussed the data and drafted the ms, SF conceived the work, performed the experiments, discussed and analyzed the data and drafted the ms.

Declaration of Competing Interest

Yolanda Ponstein and Edwin Van Amersfoort are employees of Pharming.

Appendix A. Supplementary data

Supplementary data to this article can be found online at https://doi.org/10.1016/j.bbi.2021.01.002.

References

Andjelkovic, A.V., Xiang, J., Stamatovic, S.M., Hua, Y.a., Xi, G., Wang, M.M., Keep, R.F., 2019. Endothelial targets in stroke: translating animal models to human. ATVB 39, 2240–2247. https://doi.org/10.1161/ATVBAHA.119.312816.

Beeg, M., Nobili, A., Orsini, B., Rogai, F., Gilardi, D., Fiorino, G., Danese, S., Salmona, M., Garattini, S., Gobbi, M., 2019. A Surface Plasmon Resonance-based assay to measure serum concentrations of therapeutic antibodies and anti-drug antibodies. Sci. Rep. 9 https://doi.org/10.1038/s41598-018-37950-4.

Canovi, M., Lucchetti, J., Stravalaci, M., Valentino, S., Bottazzi, B., Salmona, M., Bastone, A., Gobbi, M., 2014. A new surface plasmon resonance-based immunoassay for rapid, reproducible and sensitive quantification of pentraxin-3 in human plasma. Sensors (Basel) 14, 10864–10875. https://doi.org/10.3390/s140610864.

Carswell, H.V.O., Macrae, I.M., Farr, T.D., 2009. Complexities of oestrogen in stroke. Clin. Sci. 118, 375–389. https://doi.org/10.1042/CS20090018.

Cervera, A., Planas, A.M., Justicia, C., Urra, X., Jensenius, J.C., Torres, F., Lozano, F., Chamorro, A., 2010. Genetically-defined deficiency of mannose-binding lectin is associated with protection after experimental stroke in mice and outcome in human stroke. PLoS ONE 5, e8433. https://doi.org/10.1371/journal.pone.0008433.

Chen, X., Arumugam, T.V., Cheng, Y.-L., Lee, J.-H., Chigurupati, S., Mattson, M.P., Basta, M., 2018. Combination therapy with low-dose IVIG and a C1-esterase inhibitor ameliorates brain damage and functional deficits in experimental ischemic stroke. Neuromol. Med. 20, 63–72. https://doi.org/10.1007/s12017-017-8474-6.

Cramer, J.V., Benakis, C., Liesz, A., 2019. T cells in the post-ischemic brain: Troopers or paramedics? J. Neuroimmunol. 326, 33–37. https://doi.org/10.1016/j.jneuroim.2018.11.006.

De Blasio, D., Fumagalli, S., Longhi, L., Orsini, F., Palmioli, A., Stravalaci, M., Vegliante, G., Zanier, E.R., Bernardi, A., Gobbi, M., De Simoni, M.-G., 2017. Pharmacological inhibition of mannose-binding lectin ameliorates neurobehavioral dysfunction following experimental traumatic brain injury. J. Cereb. Blood Flow Metab. 37, 938–950. https://doi.org/10.1177/0271678X16647397.

de la Rosa, X., Cervera, A., Kristoffersen, A.K., Valdés, C.P., Varma, H.M., Justicia, C., Durduran, T., Chamorro, Á., Planas, A.M., 2014. Mannose-binding lectin promotes local microvascular thrombosis after transient brain ischemia in Mice. Stroke 45, 1453–1459. https://doi.org/10.1161/STROKEAHA.113.004111.

Denes, A., Vidyasagar, R., Feng, J., Narvainen, J., McColl, B.W., Kauppinen, R.A., Allan, S.M., 2007. Proliferating resident microglia after focal cerebral ischaemia in mice. J. Cereb. Blood Flow Metab. 27, 1941–1953. https://doi.org/10.1038/sj.jcbfm.9600495.

Du, R., Zhou, J., Lorenzano, S., Liu, W., Charoenvimolphan, N., Qian, B., Xu, J., Wang, J., Zhang, X., Wang, X., Berndt, A., Devan, W.J., Valant, V.J., Wang, J., Furie, K.L., Rosand, J., Rost, N., Friedlander, R.M., Paigen, B., Weiss, S.T., 2015. Integrative mouse and human studies implicate ANGPT1 and ZBTB7C as susceptibility genes to ischemic injury. Stroke 46, 3514–3522. https://doi.org/10.1161/STROKEAHA.115.010767.

Farrell, C., Hayes, S., Relan, A., van Amersfoort, E.S., Pijpstra, R., Hack, C.E., 2013. Population pharmacokinetics of recombinant human C1 inhibitor in patients with hereditary angioedema: Population PK of rhC1INH. Br. J. Clin. Pharmacol. 76, 897–907. https://doi.org/10.1111/bcp.12132.

Fumagalli, S., De Simoni, M.-G., 2016. Lectin complement pathway and its bloody interactions in brain ischemia. Stroke 47, 3067–3073. https://doi.org/10.1161/STROKEAHA.116.012407.

Gesuete, R., Storini, C., Fantin, A., Stravalaci, M., Zanier, E.R., Orsini, F., Vietsch, H., Mannesse, M.L.M., Ziere, B., Gobbi, M., De Simoni, M.-G., 2009. Recombinant C1 inhibitor in brain ischemic injury. Ann. Neurol. 66, 332–342. https://doi.org/10.1002/ana.21740.

Hacke, W., 2015. Interventional thrombectomy for major stroke — a step in the right direction. N. Engl. J. Med. 372, 76–77. https://doi.org/10.1056/NEJMe1413346.

Heydenreich, N., Nolte, M.W., Göb, E., Langhauser, F., Hofmeister, M., Kraft, P., Albert-Weissenberger, C., Brede, M., Varallyay, C., Göbel, K., Meuth, S.G., Nieswandt, B., Dickneite, G., Stoll, G., Kleinschnitz, C., 2012. C1-Inhibitor protects from brain ischemia-reperfusion injury by combined antiinflammatory and antithrombotic mechanisms. Stroke 43, 2457–2467. https://doi.org/10.1161/STROKEAHA.112.660340.

Krishnan, S., Lawrence, C.B., 2019. Old Dog New Tricks; Revisiting How Stroke Modulates the Systemic Immune Landscape. Front. Neurol. 10 https://doi.org/10.3389/fneur.2019.00718.

Lambertsen, K.L., Finsen, B., Clausen, B.H., 2019. Post-stroke inflammation—target or tool for therapy? Acta Neuropathol. 137, 693–714. https://doi.org/10.1007/s00401-018-1930-z.

Landsem, A., Fure, H., Mollnes, T.E., Nielsen, E.W., Brekke, O.L., 2016. C1-inhibitor efficiently delays clot development in normal human whole blood and inhibits Escherichia coli-induced coagulation measured by thromboelastometry. Thrombosis Res. 143, 63–70. https://doi.org/10.1016/j.thromres.2016.04.024.

Llovera, G., Hofmann, K., Roth, S., Salas-Pérdomo, A., Ferrer-Ferrer, M., Perego, C., Zanier, E.R., Mamrak, U., Rex, A., Party, H., Agin, V., Fauchon, C., Orset, C., Haelewyn, B., De Simoni, M.-G., Dirnagl, U., Grittner, U., Planas, A.M., Plesnila, N., Vivien, D., Liesz, A., 2015. Results of a preclinical randomized controlled

multicenter trial (pRCT): Anti-CD49d treatment for acute brain ischemia. Sci. Transl. Med. 7 https://doi.org/10.1126/scitranslmed.aaa9853, 299ra121.
Neglia, L., Fumagalli, S., Orsini, F., Zanetti, A., Perego, C., De Simoni, M.-G., 2020a. Mannose-binding lectin has a direct deleterious effect on ischemic brain microvascular endothelial cells. J. Cereb. Blood Flow Metab. 40, 1608–1620. https://doi.org/10.1177/0271678X19874509.
Neglia, L., Oggioni, M., Mercurio, D., De Simoni, M.-G., Fumagalli, S., 2020b. Specific contribution of mannose-binding lectin murine isoforms to brain ischemia/reperfusion injury. Cell Mol. Immunol. 17, 218–226. https://doi.org/10.1038/s41423-019-0225-1.
Orsini, F., Chrysanthou, E., Dudler, T., Cummings, W.J., Takahashi, M., Fujita, T., Demopulos, G., De Simoni, M.-G., Schwaeble, W., 2016. Mannan binding lectin-associated serine protease-2 (MASP-2) critically contributes to post-ischemic brain injury independent of MASP-1. J. Neuroinflammation 13. https://doi.org/10.1186/s12974-016-0684-6.
Orsini, F., Fumagalli, S., Császár, E., Tóth, K., De Blasio, D., Zangari, R., Lénárt, N., Dénes, Á., De Simoni, M.-G., 2018. Mannose-binding lectin drives platelet inflammatory phenotype and vascular damage after cerebral ischemia in mice via IL (Interleukin)-1α. Arterioscler. Thromb.. Vasc.Biol. 38, 2678–2690. https://doi.org/10.1161/ATVBAHA.118.311058.
Orsini, F., Villa, P., Parrella, S., Zangari, R., Zanier, E.R., Gesuete, R., Stravalaci, M., Fumagalli, S., Ottria, R., Reina, J.J., Paladini, A., Micotti, E., Ribeiro-Viana, R., Rojo, J., Pavlov, V.I., Stahl, G.L., Bernardi, A., Gobbi, M., De Simoni, M.-G., 2012. Targeting mannose-binding lectin confers long-lasting protection with a surprisingly wide therapeutic window in cerebral ischemia. Circulation 126, 1484–1494. https://doi.org/10.1161/CIRCULATIONAHA.112.103051.
Osthoff, M., Katan, M., Fluri, F., Schuetz, P., Bingisser, R., Kappos, L., Steck, A.J., Engelter, S.T., Mueller, B., Christ-Crain, M., Trendelenburg, M., 2011. Mannose-binding lectin deficiency is associated with smaller infarction size and favorable outcome in ischemic stroke patients. PLoS ONE 6. https://doi.org/10.1371/journal.pone.0021338 e21338.
Pannell, R., Li, S., Gurewich, V., 2015. Highly effective fibrinolysis by a sequential synergistic combination of mini-dose tPA plus low-dose mutant proUK. PLoS ONE 10. https://doi.org/10.1371/journal.pone.0122018 e0122018.
Percie du Sert, N., Alfieri, A., Allan, S.M., Carswell, H.VO., Deuchar, G.A., Farr, T.D., Flecknell, P., Gallagher, L., Gibson, C.L., Haley, M.J., Macleod, M.R., McColl, B.W., McCabe, C., Morancho, A., Moon, L.DF., O'Neill, M.J., Pérez de Puig, I., Planas, A., Ragan, C.I., Rosell, A., Roy, L.A., Ryder, K.O., Simats, A., Sena, E.S., Sutherland, B.A., Tricklebank, M.D., Trueman, R.C., Whitfield, L., Wong, R., Macrae, I.M., 2017. The IMPROVE Guidelines (Ischaemia Models: Procedural Refinements Of in Vivo Experiments). J. Cereb. Blood Flow Metab. 37, 3488–3517. https://doi.org/10.1177/0271678X17709185.
Perego, C., Fumagalli, S., De Simoni, M.-G., 2011. Temporal pattern of expression and colocalization of microglia/macrophage phenotype markers following brain ischemic injury in mice. J. Neuroinflammat. 8, 174. https://doi.org/10.1186/1742-2094-8-174.
Perego, C., Fumagalli, S., Miteva, K., Kallikourdis, M., De Simoni, M.-G., 2019. Combined genetic deletion of IL (Interleukin)-4, IL-5, IL-9, and IL-13 does not affect ischemic brain injury in mice. Stroke 50, 2207–2215. https://doi.org/10.1161/STROKEAHA.119.025196.
Schindelin, J., Arganda-Carreras, I., Frise, E., Kaynig, V., Longair, M., Pietzsch, T., Preibisch, S., Rueden, C., Saalfeld, S., Schmid, B., Tinevez, J.-Y., White, D.J., Hartenstein, V., Eliceiri, K., Tomancak, P., Cardona, A., 2012. Fiji: an open-source platform for biological-image analysis. Nat Methods 9, 676–682. https://doi.org/10.1038/nmeth.2019.
Sheriff, S., Chang, C.Y., Ezekowitz, R.A., 1994. Human mannose-binding protein carbohydrate recognition domain trimerizes through a triple alpha-helical coiled-coil. Nat. Struct. Biol. 1, 789–794. https://doi.org/10.1038/nsb1194-789.
Song, F.-Y., Wu, M.-H., Zhu, L.-H., Zhang, Z.-Q., Qi, Q.-D., Lou, C.-l., 2015. Elevated serum mannose-binding lectin levels are associated with poor outcome after acute ischemic stroke in patients with type 2 diabetes. Mol Neurobiol 52, 1330–1340. https://doi.org/10.1007/s12035-014-8941-0.
Stravalaci, M., De Blasio, D., Orsini, F., Perego, C., Palmioli, A., Goti, G., Bernardi, A., De Simoni, M.-G., Gobbi, M., 2016. A new surface plasmon resonance assay for in vitro screening of mannose-binding lectin inhibitors. J. Biomol. Screen 21, 749–757. https://doi.org/10.1177/1087057116637563.
Tomasi, S., Sarmientos, P., Giorda, G., Gurewich, V., Vercelli, A., 2011. Mutant prourokinase with adjunctive C1-inhibitor is an effective and safer alternative to tPA in rat stroke. PLoS ONE 6. https://doi.org/10.1371/journal.pone.0021999 e21999.
van Doorn, M.B.A., Burggraaf, J., van Dam, T., Eerenberg, A., Levi, M., Hack, C.E., Schoemaker, R.C., Cohen, A.F., Nuijens, J., 2005. A phase I study of recombinant human C1 inhibitor in asymptomatic patients with hereditary angioedema. J. Allergy Clin. Immunol. 116, 876–883. https://doi.org/10.1016/j.jaci.2005.05.019.
Wimmer, I., Zrzavy, T., Lassmann, H., 2018. Neuroinflammatory responses in experimental and human stroke lesions. J. Neuroimmunol. 323, 10–18. https://doi.org/10.1016/j.jneuroim.2018.07.003.
Wu, M.A., Bova, M., Berra, S., Senter, R., Parolin, D., Caccia, S., Cicardi, M., 2020. The central role of endothelium in hereditary angioedema due to C1 inhibitor deficiency. Int. Immunopharmacol. 82, 106304. https://doi.org/10.1016/j.intimp.2020.106304.
Zanier, E.R., Fumagalli, S., Perego, C., Pischiutta, F., De Simoni, M.-G., 2015. Shape descriptors of the "never resting" microglia in three different acute brain injury models in mice. ICMx 3. https://doi.org/10.1186/s40635-015-0039-0.
Zhang, Z.-G., Wang, C., Wang, J., Zhang, Z., Yang, Y.-L., Gao, L.i., Zhang, X.-Y., Chang, T., Gao, G.-D., Li, L.-H., 2015. Prognostic value of mannose-binding lectin: 90-day outcome in patients with acute ischemic stroke. Mol. Neurobiol. 51, 230–239. https://doi.org/10.1007/s12035-014-8682-0.
Zhou, W., Liesz, A., Bauer, H., Sommer, C., Lahrmann, B., Valous, N., Grabe, N., Veltkamp, R., 2013. Postischemic brain infiltration of leukocyte subpopulations differs among murine permanent and transient focal cerebral ischemia models: infiltration differs among cerebral ischemia. Brain Pathol. 23, 34–44. https://doi.org/10.1111/j.1750-3639.2012.00614.x.